nature materials

ARTICLES

PUBLISHED ONLINE: 11 MAY 2014 | DOI: 10.1038/NMAT3963

Optically enhanced coherent transport in $YBa_2Cu_3O_{6.5}$ by ultrafast redistribution of interlayer coupling

W. Hu[1†], S. Kaiser[1†], D. Nicoletti[1†], C. R. Hunt[1,2†], I. Gierz[1], M. C. Hoffmann[1], M. Le Tacon[3], T. Loew[3], B. Keimer[3] and A. Cavalleri[1,4*]

Nonlinear optical excitation of infrared active lattice vibrations has been shown to melt magnetic or orbital orders and to transform insulators into metals. In cuprates, this technique has been used to remove charge stripes and promote superconductivity, acting in a way opposite to static magnetic fields. Here, we show that excitation of large-amplitude apical oxygen distortions in the cuprate superconductor $YBa_2Cu_3O_{6.5}$ promotes highly unconventional electronic properties. Below the superconducting transition temperature ($T_c = 50$ K) inter-bilayer coherence is transiently enhanced at the expense of intra-bilayer coupling. Strikingly, even above T_c a qualitatively similar effect is observed up to room temperature, with transient inter-bilayer coherence emerging from the incoherent ground state and similar transfer of spectral weight from high to low frequency. These observations are compatible with previous reports of an inhomogeneous normal state that retains important properties of a superconductor, in which light may be melting competing orders or dynamically synchronizing the interlayer phase. The transient redistribution of coherence discussed here could lead to new strategies to enhance superconductivity in steady state.

Superconductors at equilibrium exhibit two characteristic physical properties: zero d.c. resistance and the expulsion of static magnetic fields. The first of these properties manifests itself as a zero-frequency delta function in the real part of the optical conductivity $\sigma_1(\omega)$ and by a positive imaginary part $\sigma_2(\omega)$ that diverges at low frequency as $1/\omega$.

In high T_c cuprates, the layered structure gives rise to additional c axis excitations of the superfluid, with the notable appearance of one or more longitudinal Josephson plasma modes due to tunnelling of Cooper pairs between capacitively coupled superconducting planes.

In bilayer cuprates, two longitudinal Josephson plasma modes are found[1,2], reflected by two peaks in the energy loss function $-\mathrm{Im}[1/(\varepsilon_1(\omega)+i\varepsilon_2(\omega))]$. Within each family of cuprates, the longitudinal mode frequency quantifies the strength of the Josephson coupling between pairs of CuO_2 layers (Fig. 1a). In addition, a peak in the real part of the conductivity, the so-called transverse Josephson plasma mode[3] (Fig. 1a), is observed at $\omega = \omega_T$ (refs 4–10). This second mode is characterized by simultaneous out-of-phase oscillations of the Josephson plasma within and between pairs of layers, and shares spectral weight with the zero-frequency conductivity peak[11].

In the specific case of $YBa_2Cu_3O_{6.5}$, the two longitudinal Josephson plasma modes appear as reflectivity edges and as peaks in the loss function near 30 and 475 cm^{-1} (Fig. 1b). The transverse plasma mode is observed near 400 cm^{-1}, and it is strongly coupled[12] to a 320 cm^{-1} phonon from which it gains oscillator strength with decreasing temperature.

Here, we measure the transient c axis terahertz-frequency optical properties of $YBa_2Cu_3O_{6.5}$ after excitation with mid-infrared optical pulses, both below and above T_c. Mid-infrared pump pulses of ~300 fs duration, polarized along the c direction and tuned to 670 cm^{-1} frequency (~15 μm, 83 meV, ±15%), were made resonant with the infrared-active distortion shown in Fig. 1c. The 15-μm-wavelength pulses were generated by difference-frequency mixing in an optical parametric amplifier and focused onto the samples with a maximum fluence of 4 mJ cm^{-2}, corresponding to peak electric fields up to ~3 MV cm^{-1}. At these strong fields, the apical oxygen positions are driven in an oscillatory fashion[13,14] by several per cent of the equilibrium unit-cell distance (Supplementary Information).

For temperatures below and immediately above T_c, where the largest changes of the optical properties were observed, we interrogated the solid with broadband terahertz probe pulses generated by gas ionization, covering the 20 and 500 cm^{-1} frequency range. For temperatures far above T_c, smaller conductivity changes could be measured with sufficient signal-to-noise ratio only by using narrower-band pulses (20–85 cm^{-1}), generated by optical rectification in ZnTe.

The equilibrium low-frequency imaginary part of the optical conductivity $\sigma_2(\omega)$ (Fig. 1b) is positive and increasing at frequencies below 30 cm^{-1}. Note that because of the contribution from normal transport by non-condensed quasi-particles, the overall equilibrium $\sigma_2(\omega)$ does not exhibit the $1/\omega$ frequency dependence of a London superconductor. Such $1/\omega$ frequency dependence can be observed in this frequency range only by measuring differential conductivity $\Delta\sigma_2(\omega) = \sigma_2(\omega, T < T_c) - \sigma_2(\omega, T > T_c)$.

[1]Max Planck Institute for the Structure and Dynamics of Matter, 22761 Hamburg, Germany, [2]Department of Physics, University of Illinois at Urbana-Champaign, Urbana, Illinois 61801, USA, [3]Max Planck Institute for Solid State Research, 70569 Stuttgart, Germany, [4]Department of Physics, Oxford University, Clarendon Laboratory, Oxford OX1 3PU, UK. †These authors contributed equally to this work. *e-mail: andrea.cavalleri@mpsd.cfel.de

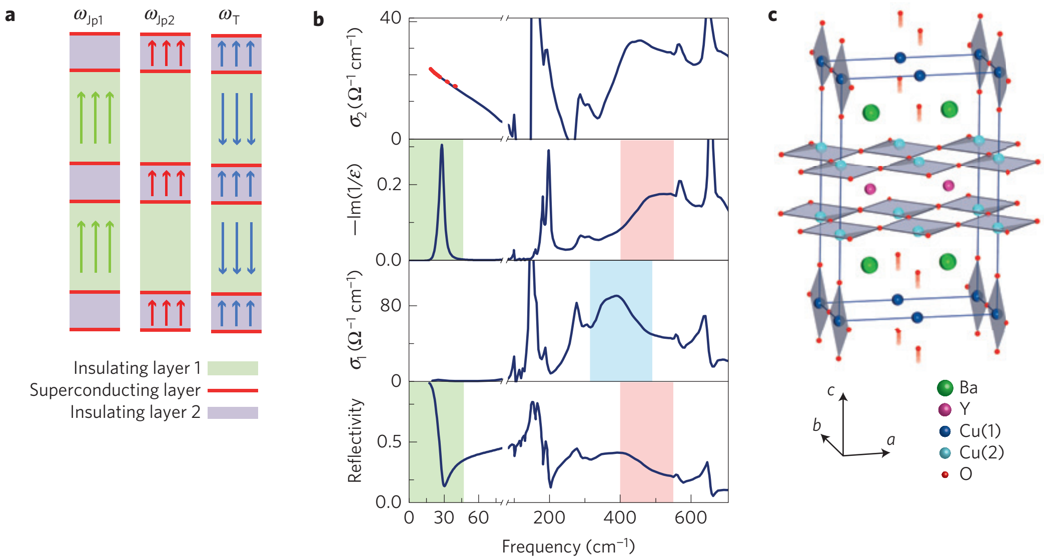

Figure 1 | Bilayer structure and *c* axis optical features in superconducting $YBa_2Cu_3O_{6.5}$. a, In the superconducting state, the structure of $YBa_2Cu_3O_{6.5}$ can be viewed as two Josephson junctions in series, which gives rise to two longitudinal modes (ω_{Jp1}, ω_{Jp2}) and a transverse mode (ω_T) (arrows indicate the direction of the current[3]). **b**, Equilibrium *c* axis optical properties for $YBa_2Cu_3O_{6.5}$ (ref. 6; the low-frequency Josephson plasma edge was characterized by narrow-band terahertz spectroscopy; see Supplementary Information). Superconductivity is evidenced by the $1/\omega$ divergence (red dashed–dotted line) in the imaginary part of the optical conductivity, $\sigma_2(\omega)$. Two longitudinal Josephson plasma modes appear as two peaks in the loss function, $-\mathrm{Im}(1/\varepsilon)$, and two edges in the reflectivity (~30 cm^{-1}, ~475 cm^{-1} shaded areas). The transverse plasma mode appears as a broad peak around 400 cm^{-1} in the real part of the optical conductivity $\sigma_1(\omega)$ (blue shaded area). **c**, Structure of $YBa_2Cu_3O_{6.5}$ (ref. 53) and sketch of the optically driven distortion for the apical oxygen. Two conducting CuO_2 planes are separated by Y atoms and form a bilayer unit. Ba atoms and the CuO_4 ribbons (Cu(1), and O in the *bc*-plane) separate bilayer units. The excitation of the infrared-active B_{1u} mode at ~15 μm (670 cm^{-1}) displaces the apical oxygen atoms along the *c* direction[54].

The broadband photoinduced response of the superconducting state of $YBa_2Cu_3O_{6.5}$ ($T = 10$ K) is reported in Figs 2 and 3. The frequency- and time-delay-dependent optical properties were extracted from measurements of the amplitude and phase of the reflected electric field after photo-excitation, using the equilibrium optical properties of the material[6] (Fig. 1b) and taking into account the pump–probe penetration depth mismatch (Supplementary Information). Immediately after excitation, a strong increase in the slope of $\sigma_2(\omega)$ was observed. As the superfluid density at equilibrium is quantified as $\omega\sigma_2(\omega)|_{\omega\to 0}$, the increase in the slope of $\sigma_2(\omega)$ suggests a transient enhancement of the superfluid density of the superconductor (see upper panel of Fig. 2a). The frequency-dependent imaginary conductivity is shown for all pump–probe time delays in the colour plot.

In Fig. 2b,c, we report the corresponding changes in the inter- and intra-bilayer coupling by plotting the time- and frequency-dependent energy-loss function $-\mathrm{Im}[1/(\varepsilon_1(\omega,\tau)+i\varepsilon_2(\omega,\tau))]$. The 30 cm^{-1} peak, which reflects the inter-bilayer longitudinal plasma mode at equilibrium, reduces in amplitude after photo excitation, as a second higher-frequency peak appears at 60 cm^{-1}. Simultaneously, the intra-bilayer peak, which at equilibrium is observed at 475 cm^{-1} (Fig. 2c), shifts to the red. All transient shifts in the loss function relax back to the equilibrium spectrum with a 7 ps exponential time constant (black dashed line in Fig. 2b,c).

Finally, Fig. 3 shows the corresponding dynamics of the real part of the conductivity $\sigma_1(\omega,\tau)$. At equilibrium, $\sigma_1(\omega)$ nears zero below 80 cm^{-1}, with several phonon peaks between 100 and 300 cm^{-1}. These phonon peaks remain virtually unaffected and only a small increase in $\sigma_1(\omega)$ is detected below 80 cm^{-1}. The strongest light-induced changes in $\sigma_1(\omega)$ are found at high frequency, where the transverse plasma mode at 400 cm^{-1} shifts to the red. Note that the redshift of this mode ($\sigma_1(\omega)$ peak at 400 cm^{-1}) is consistent with the redshift of the loss function peak at 475 cm^{-1}. The transverse mode frequency follows $\omega_T^2 = (d_2\omega_{Jp1}^2 + d_1\omega_{Jp2}^2)/(d_1+d_2)$, where d_1 and d_2 are the thickness of the inter- and intra-bilayer junctions, respectively, and ω_{Jp1} and ω_{Jp2} are the corresponding Josephson plasma frequencies. As $\omega_{Jp2} >> \omega_{Jp1}$, the change in transverse plasma mode position ω_T is dominated by ω_{Jp2}.

To analyse the photoinduced dynamics below T_c, we first note that the changes in optical properties are only partial. For example, the light-induced 60-cm^{-1} loss function peak (Fig. 2b) takes only a fraction of the equilibrium spectral weight at 30 cm^{-1}. This is interpreted as a signature of an inhomogeneous light-induced phase, in which only a fraction of the equilibrium superconducting state is being transformed, a physical situation that can be well described by Bruggeman's effective medium model[15].

$$f\,\frac{\tilde{\varepsilon}_T(\omega)-\tilde{\varepsilon}_E(\omega)}{\tilde{\varepsilon}_T(\omega)+2\tilde{\varepsilon}_E(\omega)} + (1-f)\,\frac{\tilde{\varepsilon}_S(\omega)-\tilde{\varepsilon}_E(\omega)}{\tilde{\varepsilon}_S(\omega)+2\tilde{\varepsilon}_E(\omega)} = 0$$

The effective dielectric function $\tilde{\varepsilon}_E(\omega)$ is determined here by the dielectric function $\tilde{\varepsilon}_T(\omega)$ of the photo-transformed regions, which occupy a volume fraction f, and by the dielectric function $\tilde{\varepsilon}_S(\omega)$ of the remaining $(1-f)$ volume, which we assumed to retain the properties of the equilibrium superconducting state.

The transient optical properties at all frequencies could then be fitted using a minimum number of free parameters. We considered the dielectric function $\tilde{\varepsilon}_T(\omega)$ of a second superconductor with similar optical properties to $YBa_2Cu_3O_{6.5}$ at equilibrium, but with different values of ω_{Jp1} and ω_{Jp2} and with a different 320 cm^{-1} phonon width (see Supplementary Information for details). In addition, the filling fraction f was left as a free parameter. All transient features were well reproduced by this fit, with a maximum transformed volume fraction of $f = 20\%$.

From the effective medium fit, we extract the unscreened Josephson plasma frequency for the perturbed volume fraction f. The unscreened inter-bilayer Josephson plasma frequency increases from $\omega_{Jp1} = 110$ to 310 cm^{-1}, and the unscreened intra-bilayer Josephson plasma frequency decreases from $\omega_{Jp2} = 1{,}030$ to 950 cm^{-1}, conserving the total coherent weight,

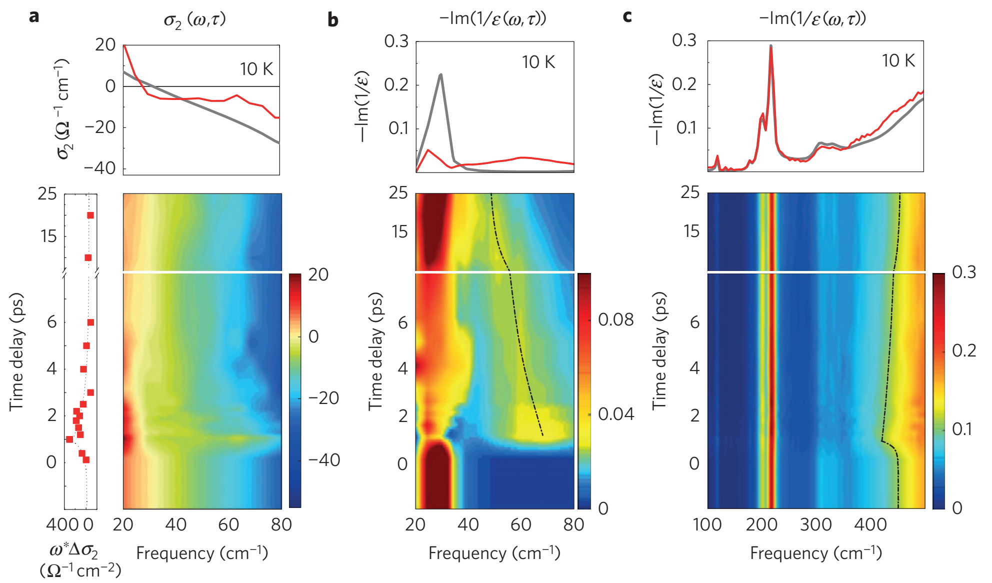

Figure 2 | Transient imaginary conductivity at low frequencies and broadband loss function response at 10 K ($T < T_c$). a, Imaginary part of the optical conductivity $\sigma_2(\omega,\tau)$. **b**, The energy loss function $-\mathrm{Im}(1/\varepsilon(\omega,\tau))$ of $YBa_2Cu_3O_{6.5}$ at low frequencies (<80 cm^{-1}). **c**, The energy loss function at high frequencies (100–475 cm^{-1}). Upper panels: Transient optical constants at maximum response (red), and the equilibrium values (grey). Lower panels: Transient optical constants as a function of frequency and time delay. The prompt increase of the $\sigma_2(\omega)$ slope is followed by a decay back to equilibrium within a few picoseconds, as shown in the one-dimensional plot on the left-hand side of the colour plot in **a**, reporting $\omega\Delta\sigma_2(\omega,\tau)$ for $\omega = 20$ cm^{-1}. A splitting of the low-frequency inter-bilayer Josephson plasma mode (~30 cm^{-1}) and a redshift of the high-energy intra-bilayer Josephson plasma mode (~475 cm^{-1}) can be seen in the energy loss function. The decay of both the low- and the high-frequency plasma modes back to equilibrium follow the same exponential decay of 7 ps (dashed–dotted lines).

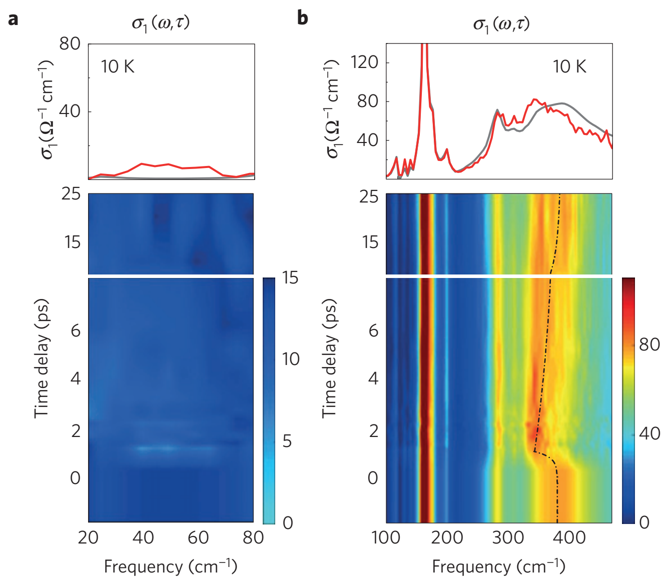

Figure 3 | Transient real part of the conductivity of $YBa_2Cu_3O_{6.5}$ at $T = 10$ K ($T < T_c$). Upper panels: Equilibrium (grey) and photoexcited real part of the optical conductivity $\sigma_1(\omega)$ at maximum transient response (red). A small contribution below 80 cm^{-1} in the low-frequency $\sigma_1(\omega)$ (**a**), and a redshift of the transverse plasmon around 400 cm^{-1} (**b**) are seen at maximum transient response. Lower panels: Photoexcited $\sigma_1(\omega)$ at various time delays. The light-induced redshift of the 400 cm^{-1} mode follows the same 7 ps exponential decay (dashed–dotted line) as the transient changes in the two Josephson plasma modes in the loss function (Fig. 2b,c).

which scales with $\omega_{\mathrm{Jp1}}^2 + \omega_{\mathrm{Jp2}}^2$. (Note that the position of the Josephson plasma edges in the reflectivity, and the peaks in the loss function are located at frequencies much smaller than ω_{Jp1} and ω_{Jp2}. Here the edge/peak positions are determined by the screened plasma frequency $\widetilde{\omega_{\mathrm{Jp}}} = \omega_{\mathrm{Jp}}/\sqrt{\varepsilon_\infty}$, with $\varepsilon_\infty = 4.5$. The interband contribution shifts the peak/edge positions further to even lower frequencies than $\widetilde{\omega_{\mathrm{Jp}}}$.)

We next turn to the response immediately above T_c, for which the signal was still large enough to allow for measurements with the same broadband source. Figure 4a shows the equilibrium and light-induced $\sigma_2(\omega)$ for $T = 60$ K ($> T_c = 50$ K). We observe a short-lived enhancement of the low-frequency σ_2, which becomes positive and increases with decreasing frequency. Note that this transient $\sigma_2(\omega)$ is very similar to that of the equilibrium superconductor at 10 K (grey line in Fig. 2a). Figure 4b,c shows the corresponding loss function. The appearance of a broad loss function peak at 55 cm^{-1}, absent in the normal state, reflects the emergence of a longitudinal plasma mode[16] approximately at the same frequency where the blueshifted mode was observed below T_c. Furthermore, the 475 cm^{-1} loss function peak (Fig. 4c) and the 400 cm^{-1} peak in σ_1 (Fig. 4e) both shift to the red, identifying a clear analogy between the below-T_c and above-T_c data. These broadband data at 60 K were also successfully fitted with the same effective medium model, where the unscreened inter-bilayer plasma frequency increases from $\omega_{\mathrm{Jp1}} = 0$ cm^{-1} to $\omega'_{\mathrm{Jp1}} = 250$ cm^{-1}, and the unscreened intra-bilayer Josephson plasma frequency $\omega_{\mathrm{Jp2}} = 1{,}030$ cm^{-1} reduces to $\omega'_{\mathrm{Jp2}} = 960$ cm^{-1} (Supplementary Information), again conserving the total coherent weight $\omega_{\mathrm{Jp1}}^2 + \omega_{\mathrm{Jp2}}^2$.

The response over a broader range of temperatures below and above T_c was measured with narrowband terahertz pulses, which were more sensitive to smaller changes in optical properties. Figure 5 shows three representative sets of results at 10, 100 and 300 K, as extracted from the experiment using the same procedure as for the broadband data. The 10 K results confirm the photoinduced enhancement in σ_2 (ω) (Fig. 5a) and a weak increase in σ_1 (ω) (Fig. 5d). For comparison, the differential measurement of the redshift in σ_1 (ω) near 400 cm^{-1} (extracted from the broadband measurements of Fig. 3b) is shown in Fig. 5g.

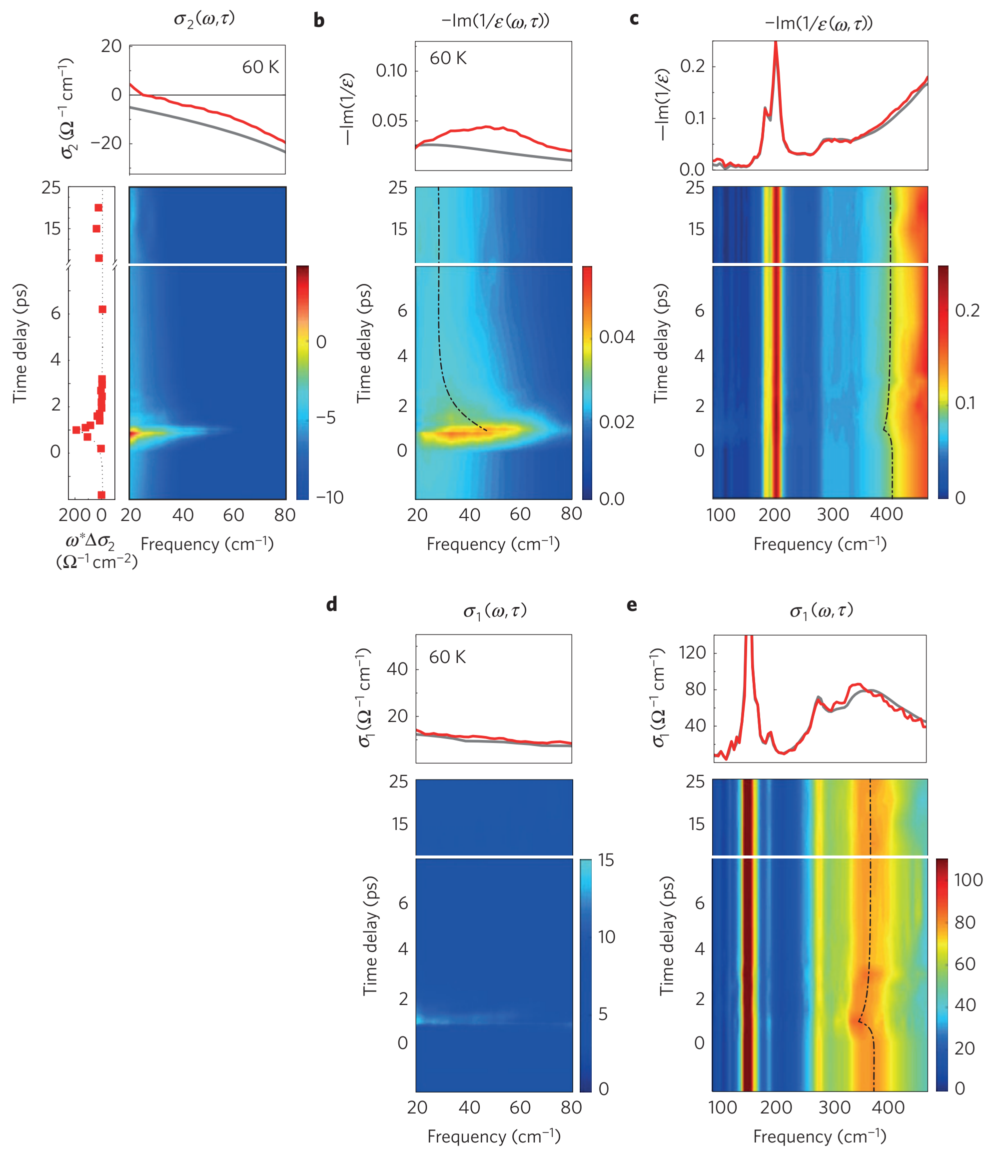

Figure 4 | Transient optical properties above T_c (at $T = 60$ K). a, Imaginary part of the optical conductivity $\sigma_2(\omega,\tau)$. An enhancement between 20 to 80 cm^{-1}, and a $1/\omega$-like divergence at low frequencies is seen in σ_2. **b**,**c**, Loss function $-\mathrm{Im}(1/\varepsilon(\omega,\tau))$ at low (**b**) and at broadband (**c**) frequencies. The equilibrium loss function is featureless below 80 cm^{-1}, and shows a strong peak at 475 cm^{-1}. On mid-infrared pumping, a peak at 55 cm^{-1} develops, indicating photoinduced inter-bilayer coherence. At higher frequencies, a redshift of the 475 cm^{-1} intra-bilayer plasmon is seen. **d**,**e**, Real part of the optical conductivity $\sigma_1(\omega,\tau)$ at low (**d**) and at broadband (**e**) frequencies. A redshift of the 400 cm^{-1} transverse plasma mode is observed. See Supplementary Information for details on the lifetime of the state above T_c.

Above T_c, at 100 K (Fig. 5b,e,h) we also observe an increase in $\sigma_2(\omega)$ that becomes positive below 30 cm^{-1}, as already shown for the 60 K data of Fig. 4a. The corresponding changes in the low-frequency $\sigma_1(\omega)$ are negligible (Fig. 5e), and a transfer of spectral weight from the 400 cm^{-1} mode to lower frequencies is detected. At 300 K (Fig. 5c,f,i), smaller changes with similar qualitative characteristics are observed. The conductivity response discussed in Fig. 5a–i is complemented by plots of reflectivity and loss function, reported in Fig. 5j–o. These figures evidence the appearance of a clear longitudinal plasma mode at $\sim$60 cm^{-1}. By fitting the temperature-dependent photoinduced enhancement $\omega\Delta\sigma_2|_{\omega\to 0}$ with an empirical mean-field law of the type $\propto\sqrt{1-(T/T')}$, a temperature scale $T' = 310\pm 10$ K is extracted for the disappearance of the effect (Fig. 5p).

We next turn to a critical discussion of all the experimental results reported above. Below T_c, we observe strengthening of the low-frequency inter-bilayer coupling, occurring at the expense of that within the bilayers. A change in the Josephson coupling strength in cuprates may be ascribed to more than one physical origin. For example, the dynamical coupling between the layers may change because the charging energy of the planes is modified. However, if this were the case, both plasma modes below T_c should shift in the same direction, that is, to lower/higher frequencies if the electronic compressibility[3] increased/decreased. Similarly, a reduction or increase of the interlayer coupling, either by ionization of the condensate across the gap or by an increase in the total number of Cooper pairs, would lead to a shift of the longitudinal modes in the same direction, either to the red or to the blue. As $\omega_{\mathrm{Jp1}}^2+\omega_{\mathrm{Jp2}}^2$ is constant throughout the dynamics, we conclude that the light only rearranges the relative tunnelling strengths, with coherence being transferred from the bilayers to the inter-bilayer region. This is further supported by a partial sum rule analysis for $\sigma_1(\omega)$ over the measured spectral range. We compare the reduction in the spectral weight at finite frequencies (20–500 cm^{-1}),

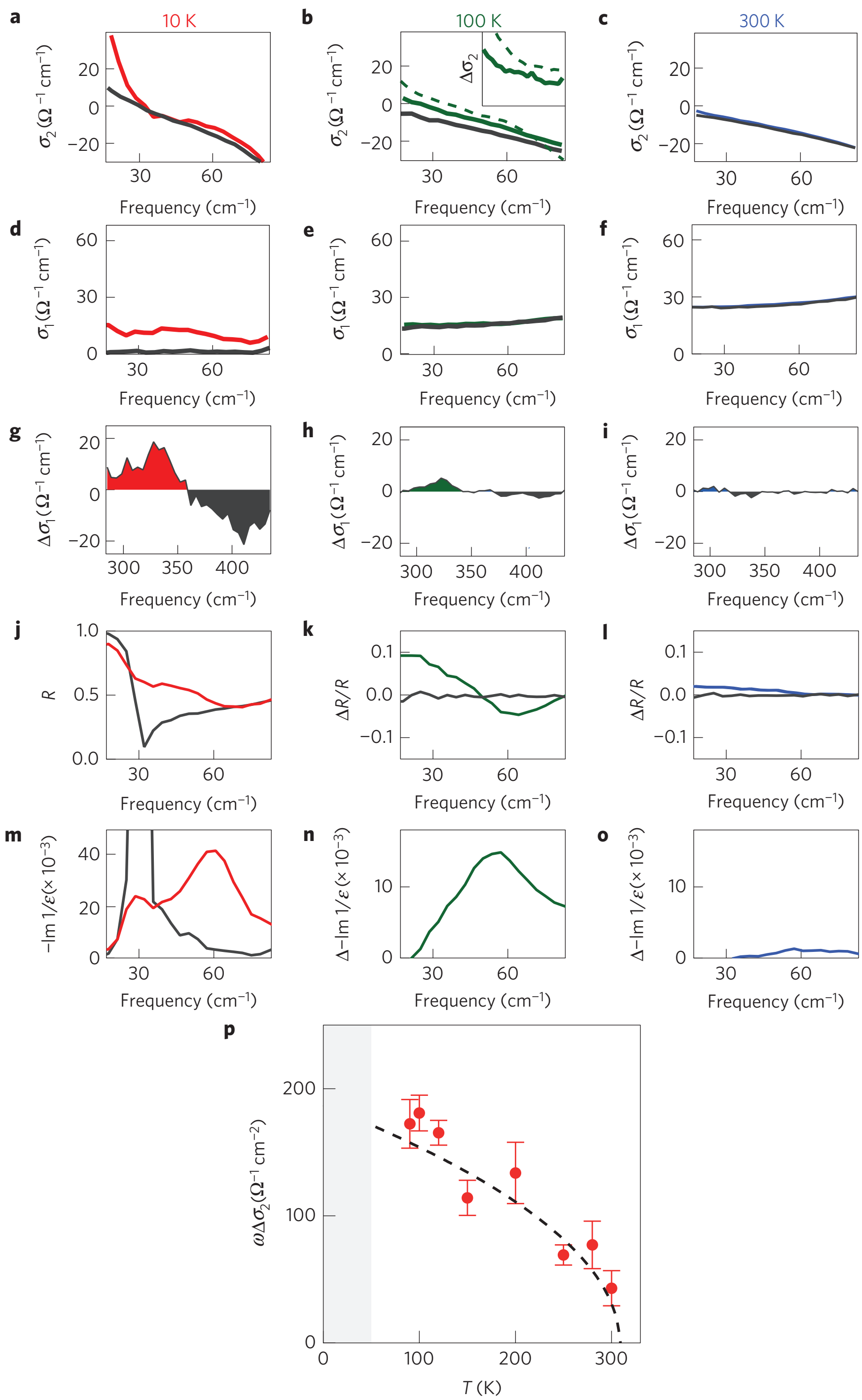

Figure 5 | Low-frequency transient optical properties below and far above T_c. a–c, Imaginary part of the conductivity $\sigma_2(\omega)$ at maximum transient response for 10 K ($T<T_c$; red), 100 K (dark green) and 300 K (blue). Grey lines, σ_2 at equilibrium. The dashed line in **b** shows the equilibrium σ_2 at 10 K ($<T_c$). The inset shows the transient change $\Delta\sigma_2=\sigma_2(\omega,\text{transient})-\sigma_2^0(\omega,\text{equilibrium})$ (solid line) compared with the equilibrium conductivity change by decreasing temperature: $\Delta\sigma_2(\omega,\Delta T)=\sigma_2^0(\omega,10\,\text{K})-\sigma_2^0(\omega,60\,\text{K})$ (dashed line). **d–f**, Real part of the conductivity $\sigma_1(\omega)$ measured at maximum transient response for 10 K ($T<T_c$), 100 K and 300 K. Grey lines, equilibrium σ_1. **g–i**, Photoinduced change $\Delta\sigma_1$ due to the redshift of the transverse plasma mode. **j**,**m**, Below T_c the reduction of the equilibrium Josephson plasma mode can be found in the reflectivity (**j**) and the loss function (**m**), and a new plasma mode is seen at $\sim$55 cm^{-1}. **k**,**l**,**n**,**o**, Differential changes in reflectivity at 100 K (**k**) and 300 K (**l**). Changes in the loss function at 100 K (**n**) and 300 K (**o**). **p**, Photoinduced enhancement $\omega\Delta\sigma_2|_{\omega\to 0}$ as a function of temperature. The dashed curve is a fit obtained with an empirical mean field dependence of the type $\propto\sqrt{1-(T/T')}$. The error bars indicate the standard deviation from the mean $\omega^{\star}\Delta\sigma_2(\omega)$ in the region between 20 and 50 cm^{-1}.

which is dominated by the ω_T peak, with the enhancement at low frequency. The zero-frequency peak, proportional to the superfluid density, cannot be measured directly in $\sigma_1(\omega)$ but can be quantified either by $\omega\sigma_2(\omega)$ for $\omega\to 0$ or, equivalently, as $\omega^2_{\text{Jp1}}\omega^2_{\text{Jp2}}/\omega^2_T$ (refs 8,12). As $\omega^2_{\text{Jp2}}\approx\omega^2_T$, the c axis superfluid density is approximately proportional to ω^2_{Jp1}, which increases after photo-excitation, thus indicating an enhancement of the superfluid density. The spectral weight loss in the light-induced state, computed as $120/\pi \int_0^{\omega_m}(\sigma_{1T} - \sigma_1^{\text{Equilibrium}})d\omega = -1.0 \times 10^5\ \text{cm}^{-2}$ (here σ_{1T} is the optical conductivity of the photo-perturbed region, and $\omega_m = 500\,\text{cm}^{-1}$ is the cutoff frequency, which is the highest frequency we could access experimentally), is comparable to the enhancement of the inter-bilayer coherence $\Delta\omega_{\text{Jp1}}^2 = 8.4 \times 10^4\,\text{cm}^{-2}$ of the same photo-perturbed region. Thus, the weakening of the intra-bilayer coupling alone seems to be responsible for the observed enhancement in superfluid density. In agreement with the below T_c case, the finite-energy sum rule for the broadband data above T_c (at $T = 60$ K) shows the spectral weight loss in σ_1 is $-7 \times 10^4\,\text{cm}^{-2}$, and the emergence of inter-bilayer coherence is $\Delta\omega_{\text{Jp1}}^2 = 6 \times 10^4\,\text{cm}^{-2}$ for the photo-perturbed region ($f = 19\%$).

Our effective medium analysis also shows that the phonon at $320\,\text{cm}^{-1}$, which is strongly coupled to the transverse Josephson plasma mode, is sharpened after excitation (Supplementary Information). Thus, rearrangement of the lattice may explain the transfer of coupling strengths between the two 'junctions'. In the same spirit of the pair-density wave interpretation of quenched Josephson coupling in stripe-ordered cuprates[17], which posits disruptively interfering tunnelling between coupled planes, one explanation of the present data may be that the relative strength of inter and intra-bilayer coupling at equilibrium is affected by interference effects caused by charge order in the planes. If charge order were perturbed at constant superfluid density, one tunnelling strength may increase at the expense of the other.

In the above T_c broadband data, a qualitative similarity to the spectral redistributions observed below T_c is found. Most conservatively, the experimental data could be fitted by the optical properties of a Drude metal with a very long scattering time $\tau_s \sim 7$ ps (corresponding to the lifetime of the state, see also Supplementary Information). This value of τ_s implies a d.c. mobility $\mu = (e\tau)/m \sim 10^3 - 10^4\,\text{cm}^2\,\text{V}^{-1}\,\text{s}^{-1}$ (depending on the carrier effective mass). Note that such high mobility would be highly unusual for incoherent transport in oxides. Furthermore, as the position of the edge does not move with the number of absorbed photons and only the fraction of material that is switched is a function of laser field, the results are hardly compatible with above-gap photoconductivity.

A more exotic effect that may give rise to extraordinarily high mobility and an anomalous dependence on the laser field may be conduction by a sliding one-dimensional charge density wave[18] (CDW). If a non-commensurate CDW in this density range[19] were to become de-pinned when the lattice is modulated, and if such a wave could slide along the c axis, it may pin again only a few picoseconds after excitation. Yet, it seems unlikely that the same carrier density as in the equilibrium superconducting state should contribute to such a CDW conductor.

An interpretation based on transient superconducting coherence induced far above T_c is in our view the most plausible. First, the photoinduced change in the imaginary conductivity $\Delta\sigma_2(\omega)$ tracks very well the change $\Delta\sigma_2(\omega) = \sigma_2(\omega, 10\,\text{K}) - \sigma_2(\omega, 60\,\text{K})$ measured at equilibrium when cooling below T_c (see inset in Fig. 5b). Second, the photoinduced plasma edge is very close to the equilibrium inter-bilayer Josephson plasma resonance, showing that light-induced transport above T_c involves a density of charge carriers very similar to the density of Cooper pairs that tunnel between the planes in the equilibrium superconductor.

Transient superconducting coherence could not be caused by quasi-particle photo-excitation[20–22], which was shown in the past to increase T_c at microwave[23–27] or optical[28,29] frequencies as the enhancement was only observed here when the pump was tuned to the phonon resonance (Supplementary Information). Rather, the nonlinear excitation of the lattice may create a displaced crystal structure[30,31] with atomic positions more favourable to high-temperature superconductivity, for example 'melting'[32,33] an ordered state[34–36] that competes with superconductivity[37] or cause a displacement of the apical oxygen away from the planes[38–42].

Similarly to what was discussed for the below-T_c data, the entire gain of coherent spectral weight above T_c can be accounted for by considering the redshift of the transverse plasma mode near $400\,\text{cm}^{-1}$. The appearance of this mode above equilibrium T_c has been discussed in the past as a signature of residual intra-bilayer superfluid density[43] in the normal state, and we speculate that redistribution of intra-bilayer coherence may explain our data.

We also mention the possibility that the observed effects result from dynamical stabilization[44–46] of superconducting phases. As the 15-μm modulation used here occurs at frequencies that are high compared with plasma excitations between planes, one could envisage a dynamically stabilized stack of Josephson junctions[47], by direct coupling of the oscillatory field to the order parameter.

We have shown that light stimulation redistributes interlayer Josephson coupling in the superconducting state of bilayer $YBa_2Cu_3O_{6.5}$, enhancing inter-bilayer coupling at the expense of the coupling within the bilayers. Above T_c, a similar phenomenology is observed, including a positive dynamical inductance, a reflectivity edge and a redistribution of spectral weight from high to low frequencies. The hypothesis of transient superconducting coupling surviving to room temperature would imply that pre-existing coherence is redistributed. This last scenario poses stringent constraints on our understanding of the normal state[48–52], and may lead to strategies for the creation of higher-temperature superconductivity over longer timescales, in driven steady state or even by designing appropriate crystal structures.

Received 18 October 2013; accepted 28 March 2014; published online 11 May 2014

References

1. Anderson, P. W. Interlayer tunneling mechanism for high-Tc superconductivity: Comparison with c axis infrared experiments. *Science* **268,** 1154–1155 (1995).
2. Shibata, H. & Yamada, T. Double Josephson plasma resonance in T* phase $SmLa_{1-x}Sr_xCuO_{4-\delta}$. *Phys. Rev. Lett.* **81,** 3519–3522 (1998).
3. van der Marel, D. & Tsvetkov, A. A. Transverse-optical Josephson plasmons: Equations of motion. *Phys. Rev. B* **64,** 024530 (2001).
4. van der Marel, D. & Tsvetkov, A. Transverse optical plasmons in layered superconductors. *Czech. J. Phys.* **46,** 3165–3168 (1996).
5. Shah, N. & Millis, A. J. Superconductivity, phase fluctuations and the c-axis conductivity in bi-layer high temperature superconductors. *Phys. Rev. B* **65,** 024506 (2001).
6. Homes, C. C. *et al.* Optical properties along the c-axis of $YBa_2Cu_3O_{6+x}$, for $x = 0.50 \rightarrow 0.95$ evolution of the pseudogap. *Physica C* **254,** 265–280 (1995).
7. Timusk, T. & Homes, C. C. The role of magnetism in forming the c-axis spectral peak at $400\,\text{cm}^{-1}$ in high temperature superconductors. *Solid State Commun.* **126,** 63–69 (2003).
8. Kakeshita, T. *et al.* Transverse Josephson plasma mode in T* cuprate superconductors. *Phys. Rev. Lett.* **86,** 4140–4143 (2001).
9. Dulić, D. *et al.* Observation of the transverse optical plasmon in $SmLa_{0.8}Sr_{0.2}CuO_{4-\delta}$. *Phys. Rev. Lett.* **86,** 4144–4147 (2001).
10. Hirata, Y. *et al.* Correlation between the interlayer Josephson coupling strength and an enhanced superconducting transition temperature of multilayer cuprate superconductors. *Phys. Rev. B* **85,** 054501 (2012).
11. Chaloupka, J., Bernhard, C. & Munzar, D. Microscopic gauge invariant theory of the c-axis infrared response of bi-layer cuprate superconductors and the origin of the superconductivity-induced absorption bands. *Phys. Rev. B* **79,** 184513 (2009).
12. Munzar, D. *et al.* Anomalies of the infared-active phonons in underdoped $YBa_2Cu_3O_y$ as an evidence for the intra-bilayer Josephson effect. *Solid State Commun.* **112,** 365–369 (1999).
13. Rini, M. *et al.* Control of the electronic phase of a manganite by mode-selective vibrational excitation. *Nature* **449,** 72–74 (2007).
14. Caviglia, A. D. *et al.* Ultrafast strain engineering in complex oxide heterostructures. *Phys. Rev. Lett.* **108,** 136801 (2012).
15. Choy, T. C. *Effective Medium Theory: Principles and Applications* (Oxford Univ. Press, 1999).
16. Huber, R. *et al.* How many-particle interactions develop after ultrafast excitation of an electron-hole plasma. *Nature* **414,** 286–289 (2001).
17. Berg, E. *et al.* Dynamical layer decoupling in a stripe-ordered high-T_c superconductor. *Phys. Rev. Lett.* **99,** 127003 (2007).

18. Grüner, G. *Density Waves in Solids* (Addison-Wesley, 1994).
19. Blanco-Canosa, S. *et al.* Momentum-dependent charge correlations in $YBa_2Cu_3O_{6+\delta}$ superconductors probed by resonant X-ray scattering: Evidence for three competing phases. *Phys. Rev. Lett.* **110,** 187001 (2013).
20. Eliashberg, G. M. Film superconductivity stimulated by a high-frequency field. *JETP Lett.* **11,** 114–116 (1970).
21. Ivlev, B. I. & Eliashberg, G. M. Influence of nonequilibrium excitations on the properties of superconducting films in a high-frequency field. *JETP Lett.* **13,** 333–336 (1971).
22. Owen, C. S. & Scalapino, D. J. Superconducting state under the influence of external dynamic pair breaking. *Phys. Rev. Lett.* **28,** 1559–1561 (1972).
23. Anderson, P. W. & Dayem, A. H. Radio-frequency effects in superconducting thin film bridges. *Phys. Rev. Lett.* **13,** 195–197 (1964).
24. Wyatt, A. F. G. *et al.* Microwave-enhanced critical supercurrents in constricted tin films. *Phys. Rev. Lett.* **16,** 1166–1169 (1966).
25. Dayem, A. H. & Wiegand, J. J. Behavior of thin-film superconducting bridges in a microwave field. *Phys. Rev* **155,** 419–428 (1967).
26. Escudero, R. & Smith, H. J. T. Energy-gap enhancement in superconducting tin by microwaves. *Phys. Rev. B* **31,** 2725–2728 (1985).
27. Beck, M. *et al.* Transient increase in the energy gap of superconducting NbN thin films excited by resonant narrowband TeraHertz pulses. *Phys. Rev. Lett.* **110,** 267003 (2013).
28. Yu, G. *et al.* Transient photoinduced conductivity in single crystals of $YBa_2Cu_3O_{6.3}$: 'Photodoping' to the metallic state. *Phys. Rev. Lett.* **67,** 2581–2584 (1991).
29. Nieva, G. *et al.* Photo-induced enhancement of superconductivity. *Appl. Phys. Lett.* **60,** 2159–2161 (1992).
30. Först, M. *et al.* Nonlinear phononics as an ultrafast route to lattice control. *Nature Phys.* **7,** 854–856 (2011).
31. Först, M. *et al.* Displacive lattice excitation through nonlinear phononics viewed by femtosecond X-ray diffraction. *Solid State Commun.* **169,** 24–27 (2013).
32. Först, M. *et al.* Driving magnetic order in a manganite by ultrafast lattice excitation. *Phys. Rev. B.* **84,** 241104(R) (2011).
33. Tobey, R. I. *et al.* Ultrafast electronic phase transition in $La_{1/2}Sr_{3/2}MnO_4$ by coherent vibrational excitation: Evidence for nonthermal melting of orbital order. *Phys. Rev. Lett.* **101,** 197404 (2009).
34. McElroy, K. *et al.* Coincidence of checkerboard charge order and antinodal state decoherence in strongly underdoped superconducting $Bi_2Sr_2CaCu_2O_{8+\delta}$. *Phys. Rev. Lett.* **94,** 197005 (2005).
35. Wu, T. *et al.* Magnetic-field-induced charge-stripe order in the high temperature superconductor $YBa_2Cu_3O_y$. *Nature* **477,** 191–194 (2011).
36. Ghiringhelli, G. *et al.* Long-range incommensurate charge fluctuations in $(Y,Nd)Ba_2Cu_3O_{6+x}$. *Science* **337,** 821–825 (2012).
37. Fausti, D. *et al.* Light induced superconductivity in a striped ordered cuprate. *Science* **331,** 189–191 (2011).
38. Pavarini, E. *et al.* Band-structure trend in hole-doped cuprates and correlation with $T_{c,\max}$. *Phys. Rev. Lett.* **87,** 047003 (2001).
39. Weber, C., Haule, K. & Kotliar, G. Apical oxygens and correlation strength in electron- and hole-doped copper oxides. *Phys. Rev. B* **82,** 125107 (2010).
40. Slezak, J. A. *et al.* Imaging the impact on cuprate superconductivity of varying the interatomic distances within individual crystal unit cells. *Proc. Natl Acad. Sci. USA* **105,** 3203–3208 (2008).
41. Mori, M. *et al.* Origin of the spatial variation of the pairing gap in Bi-based high temperature cuprate superconductors. *Phys. Rev. Lett.* **101,** 247003 (2008).
42. Sakakibara, H. *et al.* Two-orbital model explains the higher transition temperature of the single-layer Hg-cuprate superconductor compared to that of the La-cuprate superconductor. *Phys. Rev. Lett.* **05,** 057003 (2010).
43. Dubroka, A. *et al.* Evidence of a precursor superconducting phase at temperatures as high as 180 K in $RBa_2Cu_3O_{7-\delta}$ (R = Y, Gd, Eu) superconducting crystals from infrared spectroscopy. *Phys. Rev. Lett.* **106,** 047006 (2011).
44. Kapitza, P. L. Dynamic stability of a pendulum with an oscillating point of suspension. *Zh. Eksp. Teor. Fiz.* **21,** 588–597 (1951).
45. Landau, L. D. & Lifschitz, E. M. *Mechanics* (Pergamon, 1976).
46. Overhauser, A. W. Polarization of nuclei in metals. *Phys. Rev.* **92,** 411–415 (1953).
47. Baskaran, G. *Superradiant Superconductivity*. Preprint at http://arxiv.org/abs/1211.4567 (2012).
48. Gomes, K.K. *et al.* Visualizing pair formation on the atomic scale in the high Tc superconductor $Bi_2Sr_2CaCu_2O_{8+\delta}$. *Nature* **447,** 569–572 (2007).
49. Emery, V. J. & Kivelson, S. A. Importance of phase fluctuations in superconductors with small superfluid density. *Nature* **374,** 434–437 (1995).
50. Corson, J. *et al.* Vanishing of phase coherence in underdoped $Bi_2Sr_2CaCuO_{8+\delta}$. *Nature* **398,** 221–223 (1999).
51. Xu, Z. A. *et al.* Vortex-like excitations and the onset of superconducting phase fluctuation in underdoped $La_{2-x}Sr_xCuO_4$. *Nature* **406,** 486–488 (2000).
52. Bilbro, L. S. *et al.* Temporal correlations of superconductivity above the transition temperature in $La_{2-x}Sr_xCuO_4$ probed by THz spectroscopy. *Nature Phys.* **7,** 298–302 (2011).
53. Calestani, G. & Rizzoli, C. Crystal structure of the $YBa_2Cu_3O_7$ superconductor by single-crystal X-ray diffraction. *Nature* **328,** 606–607 (1987).
54. Burns, G. *et al.* Phonons in $YBa_2Cu_3O_{7-\delta}$-type materials. *Phys. Rev. B* **37,** 5171–5174 (1988).

Acknowledgements

The authors are grateful to J. Orenstein, S. Kivelson, D. Basov, D. van der Marel, C. Bernhard, A. Leitenstorfer and L. Zhang for extensive discussions, for their many suggestions and advice on the data analysis. Technical support from J. Harms and H. Liu is acknowledged.

Author contributions

A.C. conceived the project. W.H. and I.G. performed the measurements with broadband gas source. D.N., C.R.H. and S.K. performed the narrowband measurements. W.H., C.R.H., D.N. and I.G. analysed the data and discussed results with all authors. W.H. built the mid-infrared pump–broadband terahertz probe set-up with the support of M.C.H. The mid-infrared pump–narrowband terahertz probe set-up was built by S.K. and D.N. $YBa_2Cu_3O_{6.5}$ single crystals were synthesized by T.L., with guidance from M.L.T. and B.K. The manuscript was written by A.C. together with W.H. and S.K., and with input from all authors.

Additional information

Supplementary information is available in the online version of the paper. Reprints and permissions information is available online at www.nature.com/reprints. Correspondence and requests for materials should be addressed to A.C.

Competing financial interests

The authors declare no competing financial interests.